Applied Physics Letters

RESEARCH ARTICLE | FEBRUARY 21 2023

Gain recovery dynamics in active type-II semiconductor heterostructures

F. Schäfer ; M. Stein ; J. Lorenz ; F. Dobener ; C. Ngo ; J. T. Steiner ; C. Fuchs ; W. Stolz ; K. Volz ; T. Meier ; J. Hader ; J. V. Moloney ; S. W. Koch ; S. Chatterjee

Appl. Phys. Lett. 122, 082104 (2023)
https://doi.org/10.1063/5.0128777

AIP Publishing

Applied Physics Letters ARTICLE scitation.org/journal/apl

Gain recovery dynamics in active type-II semiconductor heterostructures

Cite as: Appl. Phys. Lett. **122**, 082104 (2023); doi: 10.1063/5.0128777
Submitted: 30 September 2022 · Accepted: 9 January 2023 ·
Published Online: 21 February 2023

F. Schäfer,[1] M. Stein,[1] J. Lorenz,[1] F. Dobener,[1] C. Ngo,[2] J. T. Steiner,[2] C. Fuchs,[3] W. Stolz,[3] K. Volz,[3] T. Meier,[2] J. Hader,[4] J. V. Moloney,[4] S. W. Koch,[4,5,a)] and S. Chatterjee[1,b)]

AFFILIATIONS

[1]Institute of Experimental Physics I and Center for Materials Research (LaMa), Justus-Liebig-University Giessen, Heinrich-Buff-Ring 16, D-35392 Giessen, Germany
[2]Department of Physics, Paderborn University, Warburger Strasse 100, D-33098 Paderborn, Germany
[3]Structure & Technology Research Laboratory (WZMW), Philipps-University Marburg, Hans-Meerwein-Straße 6, D-35032 Marburg, Germany
[4]Wyant College of Optical Sciences, The University of Arizona, 1630 East University Boulevard, Tucson, Arizona 85721, USA
[5]Department of Physics and Materials Sciences Center, Philipps-Universität Marburg, Renthof 5, D-35032 Marburg, Germany

[a)]Deceased.
[b)]**Author to whom correspondence should be addressed:** sangam.chatterjee@physik.uni-giessen.de

ABSTRACT

Type-II heterostructures as active layers for semiconductor laser devices combine the advantages of a spectrally broad, temperature stable, and efficient gain with the potential for electrical injection pumping. Their intrinsic charge carrier relaxation dynamics limit the maximum achievable repetition rates beyond any constraints of cavity design or heat dissipation. Of particular interest are the initial build up of gain after high-energy injection and the gain recovery dynamics following depletion through a stimulated emission process. The latter simulates the operation condition of a pulsed laser or semiconductor optical amplifier. An optical pump pulse injects hot charge carriers that eventually build up broad spectral gain in a model (Ga,In)As/GaAs/Ga(As,Sb) heterostructure. The surplus energies of the optical pump mimic the electron energies typical for electrical injection. Subsequently, a second laser pulse tuned to the broad spectral gain region depletes the population inversion through stimulated emission. The spectrally resolved nonlinear transmission dynamics reveal gain recovery times as fast as 5 ps. These data define the intrinsic limit for the highest laser repetition rate possible with this material system in the range of 100 GHz. The experimental results are analyzed using a microscopic many-body theory identifying the origins of the broad gain spectrum.

Semiconductor lasers are presumably the most versatile, compact, and energy efficient laser light source of the present age. Their advantageous properties have opened up virtually endless applications, fulfilling the prophecy of the famous quote, "a Solution Seeking a Problem".[1] In particular, pulsed-lasers are gaining more impact across all disciplines, especially for extremely fast repetition rates. Exemplary applications include processing in materials sciences and mechanical engineering,[2,3] surgeries in life sciences,[4,5] high-speed telecom applications,[6–8] and transient spectroscopy in physical sciences,[9,10] all of which will benefit from ultrafast, high-repetition-rate semiconductor lasers. Consequently, there is a tremendous research effort to develop lasers with ultra-high repetition rates. In many cases, however, these advances are not limited by the gain dynamics of the laser medium itself, but by mode-locking mechanisms, cavity designs, or heat dissipation.[7,11] Due to its great importance, gain recovery dynamics of laser media have been studied theoretically and experimentally on quantum cascade lasers[12] and quantum dot-based laser materials.[13–19] As a result, the gain recovery dynamics of some quantum dot-based structures would allow laser repetition rates beyond 200 GHz.[20,21] Much fewer experimental studies exist for quantum well (QW) structures, the gain recovery dynamics of which are generally considered to be slower than those found in quantum dot structures.[22–24] Nevertheless, QW-based semiconductor lasers dominate in many practical applications, achieving similar maximum repetition rates and shorter pulse lengths in operation than quantum dot-based devices.[25–28] The highest fundamental laser repetition rates of QW-based lasers are in the range

of 50–100 GHz,[11,29] while those of quantum dot-based lasers are in the same order of 40 to 80 GHz.[30–32]

Since subpicosecond pulses are equally necessary for ultra-high laser repetition rates in the hundred GHz range, QW-based gain media could be promising despite their slower gain recovery. Compared to regular quantum well structures, semiconductor lasers based on type-II heterostructures show promising properties like a more flexible band structure engineering or wavelength versatility and often exhibit very broad gain spectra.[33–35] Nonetheless, in these emerging type-II QW heterostructures, the gain recovery dynamics are still entirely unexplored.[36]

In this Letter, we present the ultrafast, spectrally resolved gain dynamics typical for pulsed semiconductor lasers or semiconductor optical amplifiers before and shortly after stimulated emission processes. Experimentally, the performance during operation is mimicked by studying the subpicosecond charge carrier dynamics in an (In,Ga)As/Ga(As,Sb) heterostructure with type-II band alignment as gain medium rather than performing true in-operando experiments on processed devices. We simulate the optical response after an optical pump pulse with a microscopic theory and discuss the importance of the adjacent resonances in a type-II QW. The excellent agreement supports the validity of the intrinsic material limits, i.e., the gain recovery after depletion through stimulated emission. These studies provide the theoretical maximum rate at which further laser pulses can trigger stimulated emission in this active medium and contribute to devising guidance for optimized structure design to improve repetition rates.

The heterostructures are grown by metal-organic vapor-phase epitaxy; details of the growth are given in Ref. 37. High-resolution x-ray diffraction as well as atomic force microscopy confirm the thicknesses of 7.7 and 7.5 nm for the $Ga_{0.942}In_{0.058}As$ and the $GaAs_{0.93}Sb_{0.07}$ layers, respectively. These are separated by a GaAs interlayer of 1 nm. The 50 repetitions are separated by GaAs/GaAsP/GaAs barriers, which also provide strain compensation. A schematic of the heterostructure is shown in Ref. 38 [Fig. 1(a)].

A 100 kHz repetition rate regenerative ytterbium-doped potassium gadolinium tungstate (Yb:KGW) amplifier system provides 200 fs pulses centered around 1030 nm with a pulse energy of 20 μJ. About 75 % of the amplifier emission drive an optical parametric amplifier (OPA); the rest generates a white-light supercontinuum in a 4 mm thick sapphire crystal. The main output of the OPA provides tunable central wavelength pulses, which are compressed to about 70 fs using a prism compressor. These are tuned to spectrally overlap with the material gain in the sample mounted in a helium-cooled cold-finger cryostat that cools the sample to a fixed temperature of 6 K. A residual output of the OPA delivers pulse energies up to 5 μJ at 515 nm to optically excite the sample with a preceeding laser pulse. Here, this first excitation pulse is used to drive the sample into optical inversion. We use the additional second optical pulse from the OPA to impinge on the sample with a defined time delay and harvest the previously generated optical gain expanding the scope of conventional optical pump-optical probe experiments. All beams are focused onto the sample; the two excitation beams have spot sizes of 250 μm, while the white-light supercontinuum is focused to 140 μm. We use a wedged beam splitter in the white-light beam path to split the light into two beams. One part is focused onto the sample to probe the sample's excitation-induced absorption changes and the other part is used as a reference pulse.

The white-light supercontinuum passing through the sample and the reference pulse are simultaneously and independently analyzed using an imaging spectrometer with a 500 lines/mm grating and a Si-CCD camera utilizing separate regions of interest on the chip [see Fig. 1(a)]. The spectra of both pulses are compared and a transfer function (T_f) converts the spectrum of the reference pulse (T_{ref}) into the spectrum of the pulse transmitted through the unexcited sample. The reference path, thus, provides the spectrum of the unexcited sample at any time and is independent of fluctuations in the spectrum of the white-light, as the transfer function is determined by the optical pathway through the setup and consequently does not change in time. By adding the optical excitation, we thus simultaneously obtain the transmission through the excited sample (T_P) and the transmission through the unexcited sample (T_0). Taking into account the photoluminescence (T_{Pl}) and the scattered-light background (T_{Bg}) for both white-light beam paths at the beginning of the measurement yields the differential absorption at each time step according to

$$\Delta\alpha L = -ln\left[(T_P - T_{Pl})/(T_f \cdot (T_{ref} - T_{Bg}))\right].$$

The measurements of the transmission through the excited and the unexcited sample (via the reference path) are simultaneous and, thus, not distorted by white-light fluctuations, and each time step is measured in real time just by reading out the spectrometer. These advantages provide an extremely accurate, fast, and low-noise method to determine the differential absorption.

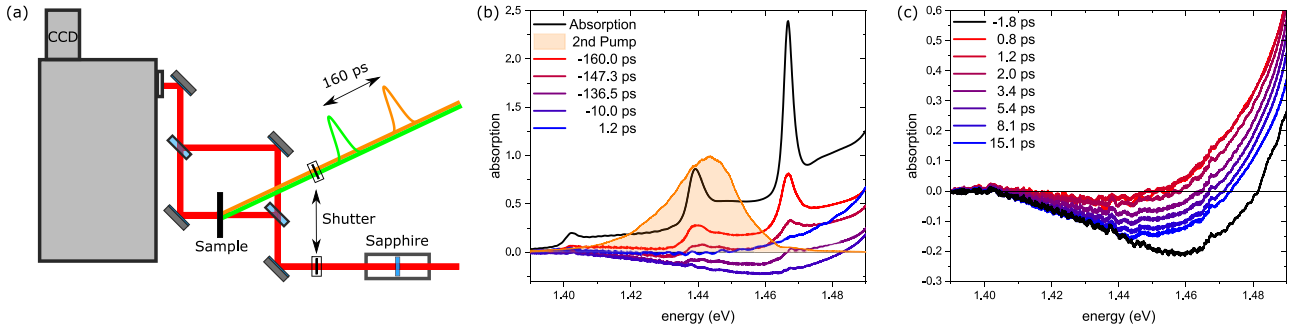

FIG. 1. (a) Schematic of the experimental optical pump—optical probe setup. The green and orange pulses have a time delay of 160 ps and are used to excite the sample, while the white-light pulses (shown as a red line) generated in the sapphire crystal probe the carrier dynamics induced by the excitation. (b) Linear absorption spectrum (black), spectrum of the second pump pulse with a central energy of 1.442 eV (orange-shaded area), and the transient absorption data for different time delays after the initial pump pulse. (c) Absorption spectra of the sample immediately before and after the second pump pulse impinges on the sample.

Adding the differential absorption to the linear absorption then yields the absorption of the excited sample, where a negative absorption corresponds to optical amplification, i.e., optical gain.

Figure 1(b) shows the linear absorption of the unexcited sample (black line). The spectrum exhibits three distinct peaks, one at 1.465 eV corresponding to the exciton peak in the (Ga,In)As layer, one at 1.440 eV representing the Ga(As,Sb) layer exciton, and one at 1.402 eV. The latter is identified as the absorption peak of the charge transfer exciton (CTX).

The times given refer to the temporal separation between the white-light pulse and the second excitation pulse that impinges on the sample at $t = 0$ ps. Excitation of the first pulse at $t = -160$ ps with 2.4 eV and a photon density of $8.9 \cdot 10^{14}/\mathrm{cm}^2$ creates hot charge carriers with significant excess energy, which corresponds to typical excitation conditions in electrically pumped GaAs-based semiconductor lasers, i.e., for injection from (Al,Ga)As barriers. After excitation, the charge carriers relax toward the bandgap on a fast, subpicosecond timescale and thermalize into hot quasi-equilibrium distributions. After that the distributions cool via phonon emission leading to rising occupations at the bandgap. This leads to a continuously increasing bleaching of the absorption, eventually resulting in population inversion observable as negative absorption and, hence, optical gain at $t = -136.5$ ps. A broad optical gain is finally present at $t = -10$ ps, extending from roughly 1.40 to 1.48 eV. Thus, the gain extends from the CTX resonance to slightly above the exciton resonance associated with the (Ga,In)As layer. This describes very well the conditions prevailing when the second pulse impinges on the sample with a photon density of $8.4 \cdot 10^{14}/\mathrm{cm}^2$ at $t = 0$ ps. The second pump pulse that is used to stimulate emission is shown as an orange line with orange shading at a central energy of 1.442 eV in Fig. 1(b). The spectrum ranges approximately from 1.41 to 1.47 eV and is, therefore, spectrally overlapping with the material gain created by the first pulse. Accordingly, the second pulse is able to cause stimulated emission and reduce the population inversion.

This behavior is clearly visible in Fig. 1(c), which shows an enlarged section of the absorption spectra for times close to the arrival of the second pulse. The optical gain disappears almost entirely right after the second pulse hits the sample, as can be seen for $t = 0.8$ ps. The gain subsequently recovers on a picosecond timescale. After about 15 ps, the gain in the spectral range from 1.40 to 1.44 eV is approximately the same as the gain immediately before the arrival of the second pulse. The gain also recovers in the higher energy spectral range from 1.44 to 1.47 eV; however, it does not reach the values prior to the arrival of the second pulse. This is attributed to the refilling of the vacated states at lower energies, i.e., between 1.40 and 1.44 eV, which are populated by the relaxation of carriers occupying the transition energy range from 1.44 to 1.47 eV.

We use a fully microscopic many-body theory to analyze the experimental observations. The model solves the semiconductor Bloch equations, i.e., the equations of motion for the microscopic optical polarizations and carrier distributions to calculate the absorption and gain spectra.[39,40] Here, coherent Coulomb effects like exciton resonances, Coulomb enhancement of the continuum absorption, and density-dependent bandgap renormalizations are fully taken into account. Also, electron–electron and electron–phonon collisions are included explicitly in second Born–Markov approximation leading to quantum-Boltzmann type scattering equations. The single-particle properties are obtained by evaluating an 8×8 $\mathbf{k} \cdot \mathbf{p}$ model for the designed heterostructure to determine the band structure and the electron and hole wavefunctions.[41] Strain effects between the different layers of the semiconductor heterostructure are treated as described in Ref. 42. Deformations of the confinement potentials due to local electron–hole charge imbalances are included by solving the corresponding Poisson–Schrödinger problem. The inhomogeneous line broadening observed in the sample absorption is taken into account through a Gaussian broadening with a width of 4 meV.

This microscopic approach has shown excellent agreement with experimental findings for a wide variety of materials covering the mid-IR to the UV wavelength regimes.[43] In particular, it has been shown to be very successful in the design and analysis of type-II QW systems as investigated here.[33,44–46]

Figure 2(a) shows the theoretical absorption spectrum for various carrier densities. Similar to the experimental absorption in Fig. 1(b), the low density absorption shows three excitonic resonances at 1.46,

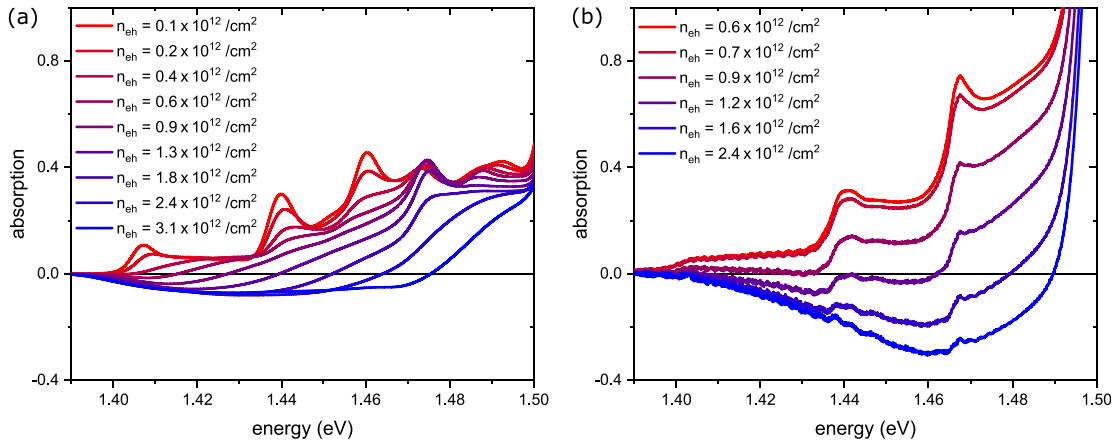

FIG. 2. (a) Theoretical absorption of the sample after optical excitation by the first pump pulse. The absorption is shown for various excitation-induced carrier densities ranging from $n_{eh} = 0.1 \cdot 10^{12}/\mathrm{cm}^2$ to $n_{eh} = 3.1 \cdot 10^{12}/\mathrm{cm}^2$. (b) Experimentally measured absorption for comparable excitation densities.

1.44, and 1.407 eV. The theory allows us to identify these as excitons where electrons and holes are both localized in the (Ga,In)As layer, both in the Ga(As,Sb) layer and where the electron is in the (Ga,In)As layer and the hole is in the Ga(As,Sb) layer, respectively. The latter represents the CTX. For high charge carrier densities of $n_{eh} = 2.4 \cdot 10^{12}/\mathrm{cm}^2$, which we obtain from a photon density of $8.9 \cdot 10^{14}/\mathrm{cm}^2$, we observe a broad gain spectrum as in the experiment in Fig. 2(b). The energetically broad gain spectrum allows for a reduced temperature sensitivity for laser and amplifier applications. In type-I QWs, the optical gain is usually dominated by the transitions between the lowest electron and hole subband since electrons and holes are localized in the same layer and the transitions have the strongest wavefunction overlap. Here, the wavefunction overlap between states in the lowest electron and hole subband is limited since the carriers are not localized in the same layer. While fewer carriers occupy the second electron and hole subbands, the overlap of these states with the energetically lowest states localized in the same layer is larger. This allows the higher subband transitions to contribute to the gain spectrum to a similar extent as the lowest subband transition leading to a spectrally wider gain—although with a somewhat lower amplitude for a given density.

The spectrally integrated transient absorption reveals detailed insights into the dynamics of the gain recovery. The transient data integrated across the energy range from 1.425 to 1.466 eV are shown in Fig. 3(a) for several photon densities of the first pump pulse. An incident photon density of $1.0 \cdot 10^{14}/\mathrm{cm}^2$ is insufficient to generate any optical gain. In this case, however, the second pulse is partially absorbed and leads to a decrease of the absorption in the sample. A photon density of $2.1 \cdot 10^{14}/\mathrm{cm}^2$ causes—on average over the integrated spectral range—a transparency in the sample as seen by the spectrally integrated absorption of zero. Higher photon densities of the first pulse generate gain in the sample. Notably, the spectrally integrated absorption is constant at values around −0.1 on a picosecond timescale before the second pump pulse hits the sample for initial pulse excitation photon densities above $3.0 \cdot 10^{14}/\mathrm{cm}^2$. The second pulse then completely dumps the spectrally integrated gain to zero, i.e., transparency is reached within the time resolution of our experiment. Unfortunately, the data recorded during the temporal overlap of the second pump pulse and the white-light pulse are obscured by two-photon absorption processes; therefore, we grayed out this time domain. The gain transiently recovers within 15 ps after the second pulse has passed the sample. The increase of the absorption at 16 ps is caused by the double pass of the second pulse reflected from the back side of the sample.

An exponential fit to the transients quantifies the recovery time constant of the gain to about 5 ps. This corresponds to the minimum time separation between two successive light pulses that can be amplified in this material system. Interestingly, this is very comparable to the gain recovery dynamics observed in type-I quantum well structures.[23,24,47] Speculations that the gain recovery is slowed down in type-II heterostructures can therefore not be confirmed experimentally.[36] Assuming that it takes about two time constants to recover a significant portion of the gain, this gives a maximum possible repetition rate of about 100 GHz. Note that our experiments are performed at liquid helium temperatures. We expect similar behavior for elevated temperatures of the crystal lattice since the relaxation dynamics at elevated excitation densities are mainly governed by Coulomb interaction rather than by phonon scattering. The calculated exponential times for several photon densities of the first pump pulse as well as the change of the absorption (step height) immediately before and after the second pulse are given in Fig. 3(b). The gain recovers slightly faster with increasing carrier densities injected by the first pulse, cf., Fig. 3(b). This can be explained by the larger reservoir of occupied states at energies above the gain region, which allows for a faster refilling. At the same time, as the excitation density of the first pulse increases, the step height, i.e., the change in absorption due to the second pulse impinging on the sample increases. Here, stronger excitations by the first pulse lead to more gain that can be depleted by the second pulse. For lower excitation densities, there is no or hardly any gain, and accordingly, the step height approaches zero. Overall, the gain recovery dynamics are quite robust for different excitation conditions. In addition, we have also performed measurements for different time delays

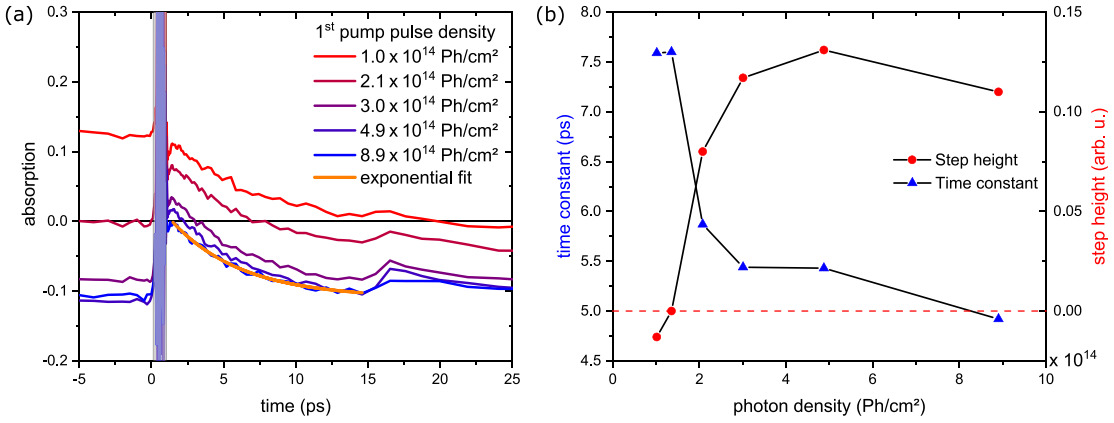

FIG. 3. (a) Spectrally integrated transients for different photon densities of the first pump pulse close to $t = 0$ ps, where the second pulse with a fixed photon density of $8.4 \cdot 10^{14}/\mathrm{cm}^2$ impinges on the sample. The second pulse depletes the gain, if present, and the subsequent gain recovery time can be extracted by an exponential fit to the transients. The temporal overlap between second pump pulse and white-light probe is grayed out due to two-photon absorption artifacts. (b) Time constants of the exponential fits together with the step height, i.e., the initial change of the absorption due to the second pulse.

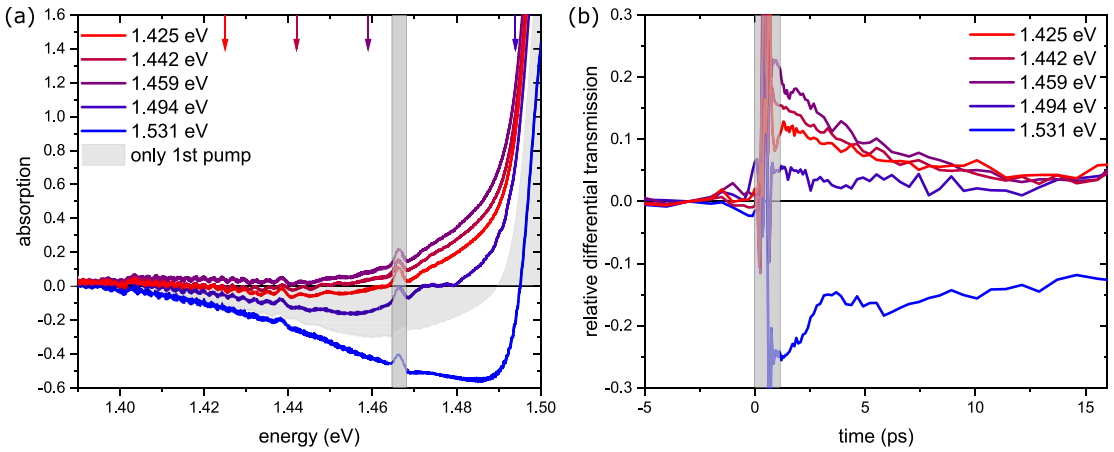

FIG. 4. (a) Gain spectra 1.5 ps after incidence of the second pulses with different central energies (indicated by arrows) on the sample. The gray shaded energy range is distorted by experimental artifacts due to strong exciton absorption at this position and the sample not being perfectly homogeneous. (b) Corresponding relative differential transmission data integrated from 1.40 to 1.49 eV. Here, the differential transmission is set to zero, shortly before the second pulse hits the sample. This allows a more direct comparison of the changes caused by the second pulses with different central energy.

between the first and the second pump pulse, ranging from 90 to 230 ps. This hardly affects the gain recovery dynamics. This corroborates the suggested similarities of the gain recovery dynamics for cw excitation or electrical injection.

In Fig. 4(a), we show the absorption spectra at 1.5 ps, i.e., shortly after the second pump pulse stimulates the sample with different central energies. Shaded in gray is the absorption spectrum at the same time delay when only the first pulse hits the sample. When the spectrum of the second pulse matches the spectral region of the material gain, the optical gain at hand is almost completely depleted. However, some gain remains when the second pulse is slightly detuned from the gain spectrum, i.e., to 1.425 eV. Larger detunings to 1.494 eV lead to far less gain depletion as the spectral overlap between the material gain and the second pulse is severely reduced. If the second pulse is detuned to 1.531 eV, i.e., into the absorptive region above the gain, the gain increases quasi-instantaneously [blue line in Figs. 4(a) and 4(b)]. This can be explained by the ultrafast thermalization of the additionally injected charge carriers close to the band edge. Since these charge carriers only have a small excess energy compared to the carriers generated by the first pulse, they do not need to cooldown for extended periods of time and, thus, immediately lead to an increase of the occupations close to the band edge.

In conclusion, the detailed gain dynamics in model type-II systems yield ultrafast gain recovery times within a few picoseconds after a stimulated emission process. These data demonstrate the physical limit to the maximum repetition rate for laser systems based on (Ga,In)As/GaAs/Ga(As,Sb) type-II heterostructures. In practice, pulsed semiconductor laser sources based on type-II multi-quantum well structures with extreme repetition rates around 100 GHz are feasible.

Financial support from the Deutsche Forschungsgemeinschaft via the Collaborative Research Center No. 223848855-SFB 1083, the European Regional Development Fund (ERDF) through the innovation laboratory high-performance materials FPG990 0005/2018, as well as the Air Force Office of Scientific Research under Award Nos. FA9550-19-1-0032 and FA9550-21-1-0463 is gratefully acknowledged.

AUTHOR DECLARATIONS

Conflict of Interest

The authors have no conflicts to disclose.

Author Contributions

Felix Schäfer: Conceptualization (equal); Data curation (equal); Formal analysis (equal); Investigation (equal); Methodology (equal); Software (equal); Visualization (equal); Writing – original draft (equal); Writing – review & editing (equal). **Torsten Meier:** Formal analysis (equal); Funding acquisition (equal); Supervision (equal); Writing – original draft (equal); Writing – review & editing (equal). **Jorg Hader:** Formal analysis (equal); Resources (equal); Software (equal); Writing – review & editing (equal). **Jerome V. Moloney:** Funding acquisition (equal); Supervision (equal); Writing – review & editing (equal). **Stephan W. Koch:** Conceptualization (equal); Funding acquisition (equal); Resources (equal); Supervision (equal). **Sangam Chatterjee:** Conceptualization (equal); Funding acquisition (equal); Methodology (equal); Project administration (equal); Resources (equal); Supervision (equal); Validation (equal); Writing – review & editing (equal). **Markus Stein:** Conceptualization (lead); Data curation (equal); Formal analysis (equal); Investigation (equal); Methodology (equal); Resources (supporting); Supervision (equal); Validation (equal); Writing – original draft (equal); Writing – review & editing (equal). **Janine Lorenz:** Data curation (supporting); Formal analysis (equal); Investigation (equal); Methodology (equal); Visualization (supporting); Writing – original draft (supporting); Writing – review & editing (equal). **Florian Dobener:** Data curation (supporting); Software (lead). **Cong Ngo:** Data curation (supporting); Formal analysis (supporting); Software (equal); Writing – review &

editing (equal). **Johannes T. Steiner:** Data curation (equal); Formal analysis (equal); Writing – original draft (equal); Writing – review & editing (equal). **Christian Fuchs:** Resources (lead). **Wolfgang Stolz:** Resources (equal); Supervision (supporting). **Kerstin Volz:** Funding acquisition (equal); Resources (lead); Supervision (supporting).

DATA AVAILABILITY

The data that support the findings of this study are available from the corresponding author upon reasonable request.

REFERENCES

[1]T. H. Maiman, "Stimulated optical radiation in ruby," Nature **187**, 493 (1960).
[2]K. C. Phillips, H. H. Gandhi, E. Mazur, and S. Sundaram, "Ultrafast laser processing of materials: A review," Adv. Opt. Photonics **7**, 684–712 (2015).
[3]M. Malinauskas, A. Žukauskas, S. Hasegawa, Y. Hayasaki, V. Mizeikis, R. Buividas, and S. Juodkazis, "Ultrafast laser processing of materials: From science to industry," Light **5**, e16133–e16133 (2016).
[4]K. E. Donaldson, R. Braga-Mele, F. Cabot, R. Davidson, D. K. Dhaliwal, R. Hamilton, M. Jackson, L. Patterson, K. Stonecipher, S. H. Yoo *et al.*, "Femtosecond laser-assisted cataract surgery," J. Cataract Refractive Surg. **39**, 1753–1763 (2013).
[5]C. L. Hoy, O. Ferhanoğlu, M. Yildirim, K. H. Kim, S. S. Karajanagi, K. M. C. Chan, J. B. Kobler, S. M. Zeitels, and A. Ben-Yakar, "Clinical ultrafast laser surgery: Recent advances and future directions," IEEE J. Sel. Top. Quantum Electron. **20**, 242–255 (2014).
[6]T. J. Kippenberg, R. Holzwarth, and S. A. Diddams, "Microresonator-based optical frequency combs," Science **332**, 555–559 (2011).
[7]A. S. Mayer, C. Phillips, and U. Keller, "Watt-level 10-gigahertz solid-state laser enabled by self-defocusing nonlinearities in an aperiodically poled crystal," Nat. Commun. **8**, 1673 (2017).
[8]V. Torres-Company, J. Schröder, A. Fülöp, M. Mazur, L. Lundberg, Ó. B. Helgason, M. Karlsson, and P. A. Andrekson, "Laser frequency combs for coherent optical communications," J. Lightwave Technol. **37**(7), 1663–1670 (2019).
[9]R. Berera, R. van Grondelle, and J. Kennis, "Ultrafast transient absorption spectroscopy: Principles and application to photosynthetic systems," Photosynth. Res. **101**, 105–118 (2009).
[10]M. Maiuri, M. Garavelli, and G. Cerullo, "Ultrafast spectroscopy: State of the art and open challenges," J. Am. Chem. Soc. **142**, 3–15 (2020).
[11]M. Mangold, C. A. Zaugg, S. M. Link, M. Golling, B. W. Tilma, and U. Keller, "Pulse repetition rate scaling from 5 to 100 GHz with a high-power semiconductor disk laser," Opt. Express **22**, 6099–6107 (2014).
[12]H. Choi, L. Diehl, Z.-K. Wu, M. Giovannini, J. Faist, F. Capasso, and T. B. Norris, "Gain recovery dynamics and photon-driven transport in quantum cascade lasers," Phys. Rev. Lett. **100**, 167401 (2008).
[13]N. Majer, K. Lüdge, and E. Schöll, "Cascading enables ultrafast gain recovery dynamics of quantum dot semiconductor optical amplifiers," Phys. Rev. B **82**, 235301 (2010).
[14]J. Gomis-Bresco, S. Dommers, V. V. Temnov, U. Woggon, M. Lämmlin, D. Bimberg, E. Malic, M. Richter, E. Schöll, and A. Knorr, "Impact of coulomb scattering on the ultrafast gain recovery in ingaas quantum dots," Phys. Rev. Lett. **101**, 256803 (2008).
[15]W. W. Chow and S. W. Koch, "Theory of semiconductor quantum-dot laser dynamics," IEEE J. Quantum Electron. **41**, 495–505 (2005).
[16]T. W. Berg, S. Bischoff, I. Magnusdottir, and J. Mork, "Ultrafast gain recovery and modulation limitations in self-assembled quantum-dot devices," IEEE Photonics Technol. Lett. **13**, 541–543 (2001).
[17]A. J. Zilkie, J. Meier, P. W. Smith, M. Mojahedi, J. S. Aitchison, P. J. Poole, C. N. Allen, P. Barrios, and D. Poitras, "Femtosecond gain and index dynamics in an InAs/InGaAsp quantum dot amplifier operating at 1.55 μm," Opt. Express **14**, 11453–11459 (2006).
[18]K. Kim, J. Urayama, T. B. Norris, J. Singh, J. Phillips, and P. Bhattacharya, "Gain dynamics and ultrafast spectral hole burning in In(Ga)As self-organized quantum dots," Appl. Phys. Lett. **81**, 670–672 (2002).
[19]B. Herzog, N. Owschimikow, J.-H. Schulze, R. Rosales, Y. Kaptan, M. Kolarczik, T. Switaiski, A. Strittmatter, D. Bimberg, U. W. Pohl *et al.*, "Fast gain and phase recovery of semiconductor optical amplifiers based on submonolayer quantum dots," Appl. Phys. Lett. **107**, 201102 (2015).
[20]S. Dommers, V. V. Temnov, U. Woggon, J. Gomis, J. Martinez-Pastor, M. Laemmlin, and D. Bimberg, "Complete ground state gain recovery after ultrashort double pulses in quantum dot based semiconductor optical amplifier," Appl. Phys. Lett. **90**, 033508 (2007).
[21]E. U. Rafailov, M. A. Cataluna, and W. Sibbett, "Mode-locked quantum-dot lasers," Nat. Photonics **1**, 395–401 (2007).
[22]A. J. Zilkie, J. Meier, M. Mojahedi, P. J. Poole, P. Barrios, D. Poitras, T. J. Rotter, C. Yang, A. Stintz, K. J. Malloy *et al.*, "Carrier dynamics of quantum-dot, quantum-dash, and quantum-well semiconductor optical amplifiers operating at 1.55 μm," IEEE J. Quantum Electron. **43**, 982–991 (2007).
[23]L. Zhang, I. Kang, A. Bhardwaj, N. Sauer, S. Cabot, J. Jaques, and D. Neilson, "Reduced recovery time semiconductor optical amplifier using p-type-doped multiple quantum wells," IEEE Photonics Technol. Lett. **18**, 2323–2325 (2006).
[24]G. Eisenstein, J. Wiesenfeld, M. Wegener, G. Sucha, D. Chemla, S. Weiss, G. Raybon, and U. Koren, "Ultrafast gain dynamics in 1.5 μm multiple quantum well optical amplifiers," Appl. Phys. Lett. **58**, 158–160 (1991).
[25]A. C. Tropper, A. H. Quarterman, and K. G. Wilcox, "Ultrafast vertical-external-cavity surface-emitting semiconductor lasers," in *Semiconductors and Semimetals* (Elsevier, 2012), Vol. 86, pp. 269–300.
[26]J. Lee, R. Oszwałdowski, C. Gøthgen, and I. Žutić, "Mapping between quantum dot and quantum well lasers: From conventional to spin lasers," Phys. Rev. B **85**, 045314 (2012).
[27]A. H. Quarterman, K. G. Wilcox, V. Apostolopoulos, Z. Mihoubi, S. P. Elsmere, I. Farrer, D. A. Ritchie, and A. Tropper, "A passively mode-locked external-cavity semiconductor laser emitting 60-fs pulses," Nat. Photonics **3**, 729–731 (2009).
[28]D. Waldburger, S. M. Link, M. Mangold, C. G. Alfieri, E. Gini, M. Golling, B. W. Tilma, and U. Keller, "High-power 100 fs semiconductor disk lasers," Optica **3**, 844–852 (2016).
[29]D. Lorenser, D. J. Maas, H. J. Unold, A.-R. Bellancourt, B. Rudin, E. Gini, D. Ebling, and U. Keller, "50-GHz passively mode-locked surface-emitting semiconductor laser with 100-mW average output power," IEEE J. Quantum Electron. **42**, 838–847 (2006).
[30]M. Laemmlin, G. Fiol, C. Meuer, M. Kuntz, F. Hopfer, A. R. Kovsh, N. N. Ledentsov, and D. Bimberg, "Distortion-free optical amplification of 20–80 GHz modelocked laser pulses at 1.3 μm using quantum dots," Electron. Lett. **42**, 697–699 (2006).
[31]G. Fiol, D. Arsenijević, D. Bimberg, A. Vladimirov, M. Wolfrum, E. Viktorov, and P. Mandel, "Hybrid mode-locking in a 40 GHz monolithic quantum dot laser," Appl. Phys. Lett. **96**, 011104 (2010).
[32]A. Zhukov, M. Maksimov, and A. Kovsh, "Device characteristics of long-wavelength lasers based on self-organized quantum dots," Semiconductors **46**, 1225–1250 (2012).
[33]C. Berger, C. Möller, P. Hens, C. Fuchs, W. Stolz, S. W. Koch, A. Ruiz Perez, J. Hader, and J. V. Moloney, "Novel type-II material system for laser applications in the near-infrared regime," AIP Adv. **5**, 047105 (2015).
[34]C. Möller, C. Fuchs, C. Berger, A. Ruiz Perez, M. Koch, J. Hader, J. V. Moloney, S. W. Koch, and W. Stolz, "Type-II vertical-external-cavity surface-emitting laser with Watt level output powers at 1.2 μm," Appl. Phys. Lett. **108**, 071102 (2016).
[35]C. Fuchs, A. Baeumner, A. Brueggemann, C. Berger, C. Moeller, S. Reinhard, J. Hader, J. V. Moloney, S. W. Koch, and W. Stolz, "Temperature-dependent spectral properties of (GaIn) As/Ga (AsSb)/(GaIn) As W-quantum well heterostructure lasers," arXiv:2012.01522 (2020).
[36]I. Kilen, S. W. Koch, J. Hader, and J. Moloney, "Mode-locking in vertical external-cavity surface-emitting lasers with type-II quantum-well configurations," Appl. Phys. Lett. **114**, 252102 (2019).
[37]M. Stein, C. Lammers, P.-H. Richter, C. Fuchs, W. Stolz, M. Koch, O. Vänskä, M. J. Weseloh, M. Kira, and S. W. Koch, "Dynamics of charge-transfer excitons in type-II semiconductor heterostructures," Phys. Rev. B **97**, 125306 (2018).

[38]M. Fey, M. Stein, C. Fuchs, W. Stolz, K. Volz, and S. Chatterjee, "Phase relaxation control in heterostructures featuring charge-transfer excitons," Phys. Rev. B **106**, 165303 (2022).
[39]M. Kira and S. W. Koch, *Semiconductor Quantum Optics* (Cambridge University Press, 2011).
[40]H. Haug and S. W. Koch, *Quantum Theory of the Optical and Electronic Properties of Semiconductors* (World Scientific Publishing Company, 2009).
[41]W. W. Chow, S. W. Koch, and M. I. Sargent, *Semiconductor-Laser Physics* (Springer Science & Business Media, 2012).
[42]S. L. Chuang, "Efficient band-structure calculations of strained quantum wells," Phys. Rev. B **43**, 9649 (1991).
[43]See http://www.nlcstr.com/publications.htm and http://www.nlcstr.com/examples0.htm for more details about the microscopic approach.
[44]J. Hader, J. V. Moloney, S. W. Koch, I. Vurgaftman, and J. R. Meyer, "Microscopic analysis of mid-infrared type-II 'W' diode lasers," Appl. Phys. Lett. **94**, 061106 (2009).
[45]C. Fuchs, C. Berger, C. Möller, M. Weseloh, S. Reinhard, J. Hader, J. V. Moloney, S. W. Koch, and W. Stolz, "Electrical injection type-II (gain) As/Ga(AsSb)/(GaIn) As single 'W'-quantum well laser at 1.2 μm," Electron. Lett. **52**, 1875–1877 (2016).
[46]C. Lammers, M. Stein, C. Berger, C. Möller, C. Fuchs, A. Ruiz Perez, A. Rahimi-Iman, J. Hader, J. Moloney, W. Stolz *et al.*, "Gain spectroscopy of a type-II VECSEL chip," Appl. Phys. Lett. **109**, 232107 (2016).
[47]S. Weiss, J. Wiesenfeld, D. Chemla, G. Raybon, G. Sucha, M. Wegener, G. Eisenstein, C. Burrus, A. Dentai, U. Koren *et al.*, "Carrier capture times in 1.5 μm multiple quantum well optical amplifiers," Appl. Phys. Lett. **60**, 9–11 (1992).